

The lowest order QED radiative corrections to longitudinally polarized Møller scattering

A. Ilyichev*

NC PHEP, 220040 Minsk, Belarus

V. Zykunov†

GSTU, 246746 Gomel, Belarus

(Dated: April 21, 2005)

The total lowest-order electromagnetic radiative corrections to the observables in Møller scattering of longitudinally polarized electrons have been calculated. The final expressions obtained by the covariant method for the infrared divergency cancellation are free from any unphysical cut-off parameters. Since the calculation is carried out within the ultrarelativistic approximation our result has a compact form that is convenient for computing. Basing on these expressions the FORTRAN code MERA has been developed. Using this code the detailed numerical analysis performed under SLAC (E-158) and JLab kinematic conditions has shown that the radiative corrections are significant and rather sensitive to the value of the missing mass (inelasticity) cuts.

PACS numbers: 13.40.Ks, 13.88.+e

I. INTRODUCTION

The present intense interest of physicists in polarized Møller scattering is stimulated by several reasons. Today the measurement of the parity-violating asymmetry A_{PV} in the recent experiment E158 [1, 2] at SLAC gives the $\sin\theta_W$ with the best precision. Further, experimentally Møller scattering is actively used in polarimetry to measure the polarization of the electron beams [3] as well as monitoring of luminosity (for example, at DESY [4]). At last, yet another reason stimulating an interest in Møller scattering consists in possibility to test the Standard Model and to reveal traces of new physics. In the intensively discussed projects of the ILC, e^-e^- and $\mu^-\mu^-$ colliders [5], high hopes for the discovery of Higgs bosons, manifestations of contact interactions, the compositeness of the electron, new gauge bosons, etc., are pinned on the scattering of identical polarized fermions (e, μ).

A precise comparison of the experimental results with the theoretical predictions requires to take into account the radiative effects correctly on both QED and electroweak levels.

Generally within the polarimetry measurements by the Møller scattering, the value of the transferred momentum is rather low, and therefore electroweak effects can usually be neglected. But otherwise in the projects of NLC where the energies are characterized by the TeV region, the value of the weak and electromagnetic effects will have the same order. Similarly, due to specific character of observables, such experiments as E-158 is sensitive to both electromagnetic and electroweak radiative corrections (and new physics phenomena at the TeV scales).

The exact calculation of the lowest-order electromagnetic radiative correction to polarized Møller scattering was performed by Shumeiko and Suarez [6]. The electroweak radiative corrections to polarized Møller scattering at high energies were computed in [7] (without hard bremsstrahlung contribution), and at low energies corresponding to conditions of E-158 were computed in papers [8] (without hard bremsstrahlung) and [9, 10] (including hard bremsstrahlung). The detailed calculation presented there demonstrates the significant value of the radiative effects that have to be explicitly included both in QED and the Electroweak theory predictions.

Similarly to [6], we perform our calculations within the covariant Bardin–Shumeiko approach [11, 12], that allows to cancel out the infrared divergences in such a way that the final result does not depend on any unphysical parameters (such as a frame-dependent cutoff ΔE that separates the soft photon contribution region from the hard one). Using the ultrarelativistic approximation allows us to obtain the compact form for radiative correction expression that is convenient (and sometimes necessary) for fast and more precise computer treatment. Moreover during the numerical estimations it was found that the numerical result strictly depends on missing mass cuts. At the same time it should be stress that the first correct application of the some kinematical cuts within the covariant Bardin–Shumeiko approach was presented in [13, 14]. Unfortunately this investigation was absent in [6].

The paper is organized as follows. In the Section II the kinematics of Møller scattering as well as the cross section at the lowest order is introduced. In the Section III the structure of the lowest order radiative corrections (virtual and real photon contributions) is explained. The Section IV presents numerical results applied to the kinematics of E-158 (SLAC) and JLab experiments. The Section V contains some conclusions. The explicit expressions for finite part of the real photon emission could be find in

*Electronic address: ily@hep.by

†Electronic address: zykunov@gstu.gomel.by

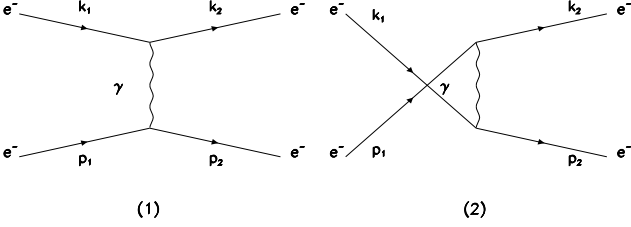


FIG. 1: The lowest order graphs giving contribution to the Møller scattering 1) t -channel; 2) u -channel.

Appendix.

II. BORN CROSS SECTION

The lowest order Feynman graphs giving the contribution to Møller scattering are presented in Fig. 1. Let us define the 4-momenta of the incoming and outgoing electrons with masses m denoted by k_1, p_1 and k_2, p_2 respectively. Then Mandelstam variables can be introduced in the standard way:

$$s = (k_1 + p_1)^2, \quad t = (k_1 - k_2)^2, \quad u = (k_2 - p_1)^2, \\ s + t + u = 4m^2. \quad (1)$$

Notice that for the Born kinematics (strictly speaking for the non radiative process)

$$u = u_0 \equiv 4m^2 - s - t. \quad (2)$$

Neglecting the electron mass, the Born cross section for the Møller scattering of longitudinal electrons can be written as follows

$$\sigma^0 = \frac{2\pi\alpha^2}{t^2} \left[(1+P) \frac{u^2}{s} - (1-P) \frac{s^2}{u} \right] + (t \leftrightarrow u), \quad (3)$$

Here and later each σ denotes the differential cross section over the kinematic variable y ($\sigma \equiv d\sigma/dy$) that is defined as

$$y = -\frac{t}{s}, \quad (4)$$

$P = P_B P_T$, where P_B, P_T are the polarizations of the beam and target electrons.

We will use the cross section subscripts L and R for $P_{B(T)} = -1$ and $P_{B(T)} = +1$ correspondingly, the first subscript corresponds to beam polarization, the second – to target polarization. The form of the Born cross section (3) with factorized combinations $1 \pm P_B P_T$ is very convenient for construction of polarization asymmetry A_{LR} that is conventionally defined as

$$A_{LR} = \frac{\sigma_{LR} - \sigma_{LL}}{\sigma_{LR} + \sigma_{LL}}. \quad (5)$$

It should be noted that on the Born level the asymmetry (5) does not depend on any energies:

$$A_{LR}^0 = \frac{y(1-y)(y^2-y+2)}{(1+y(y-1))^2} = \frac{\sin^2 \theta (7 + \cos^2 \theta)}{(3 + \cos^2 \theta)^2}, \quad (6)$$

where θ is a scattering angle of the detected electron with 4-momentum k_2 in the center mass system. The cosine of this angle can be expressed via invariants in the standard way:

$$\cos \theta = 1 + 2t/s = 1 - 2y, \quad (7)$$

while the energy of the scattering lepton in Lab. system reads:

$$E_{k_2} = \frac{s+t}{2m}. \quad (8)$$

III. ELECTROMAGNETIC RADIATIVE CORRECTIONS

The lowest order radiative corrections to Møller scattering appear from the graphs with the additional virtual particle (V-contribution, see Fig. 2 for the t -channel) and from the real photon bremsstrahlung (R-contribution, see Fig. 3 for the t -channel). It should be noted that both these parts include the infrared divergency but their sum must be infrared free. In this section the explicit expression for V- and R- contributions as well as their infrared free sum are presented.

A. Virtual contribution

For the calculation of one-loop electromagnetic radiative corrections we apply the on-shell renormalization scheme of electroweak standard model. The building blocks needed for explicit calculations according to this scheme have been worked out in paper of Böhm et al. [15], where we take the results for gauge boson self-energies and vertex functions.

The virtual contributions to Møller scattering can be separated into three parts:

$$\sigma^V = \sigma^S + \sigma^{Ver} + \sigma^{Box}, \quad (9)$$

where

1. σ^S is a virtual photon self-energy contribution (Fig. 2 (1));
2. σ^{Ver} is a vertex function contribution (Fig. 2 (2-3));
3. σ^{Box} is a box contribution (Fig. 2 (4-5)).

Now we consider each of them.

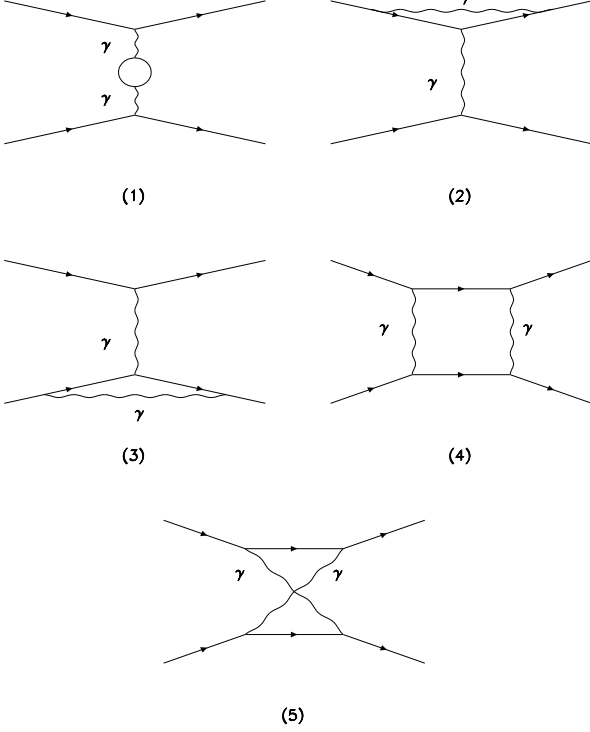


FIG. 2: The virtual one-loop graphs giving contribution to the corrected Møller scattering within t -channel.

1. The contribution of the virtual photon self energies (including the photon vacuum polarization by hadrons) to the cross section looks like

$$\sigma^S = \frac{4\pi\alpha^2}{t^2} \text{Re} \left(-\frac{1}{t} \hat{\Sigma}_T^\gamma(t) + \Pi_h(-t) \right) \times \left[(1+P) \frac{u^2}{s} - (1-P) \frac{s^2}{u} \right] + (t \leftrightarrow u). \quad (10)$$

Here $\hat{\Sigma}_T^\gamma(-t)$ is the renormalized transverse part of the γ -self-energy [15] (this part includes vacuum polarization by e , μ and τ charged leptons: in corresponding formula of [15] we should take a summing index $f = e, \mu, \tau$). Hadronic part of the photonic vacuum polarization associated with light quarks can be directly obtained from the data on process $e^+e^- \rightarrow \text{hadrons}$ via dispersion relations. Here we use parameterization of [16]

$$\text{Re}\Pi_h(-t) \cong A + B \log(1 + C|t|), \quad (11)$$

with updated parameters A,B,C in different energy regions.

2. For the contribution of electron vertices we used the results of the paper [15] (see also references

therein). We can obtain the vertex part as

$$\sigma^{Ver} = \frac{2\alpha^3}{t^2} \left[(1+P) \frac{u^2}{s} - (1-P) \frac{s^2}{u} \right] \Lambda_1(t, m^2) + (t \leftrightarrow u), \quad (12)$$

where

$$\Lambda_1(t, m^2) = -2 \log \frac{|t|}{\lambda^2} \left(\log \frac{|t|}{m^2} - 1 \right) + \log \frac{|t|}{m^2} + \log^2 \frac{|t|}{m^2} + 4 \left(\frac{\pi^2}{12} - 1 \right). \quad (13)$$

3. The box cross section reads:

$$\sigma^{Box} = \frac{2\alpha^3}{t} \left[\frac{1+P}{s} \left(\frac{2u^2}{t} \log \frac{s}{|u|} \log \frac{|su|}{\lambda^2 m^2} - \delta_{(\gamma\gamma)}^1 \right) - \frac{1-P}{u} \left(\frac{2s^2}{t} \log \frac{s}{|u|} \log \frac{|su|}{\lambda^2 m^2} - \delta_{(\gamma\gamma)}^2 \right) \right] + (t \leftrightarrow u), \quad (14)$$

The expressions $\delta_{(\gamma\gamma)}^{1,2}$ have the form:

$$\begin{aligned} \delta_{(\gamma\gamma)}^1 &= l_s^2 \frac{s^2 + u^2}{2t} - l_s u - (l_x^2 + \pi^2) \frac{u^2}{t}, \\ \delta_{(\gamma\gamma)}^2 &= l_s^2 \frac{s^2}{t} + l_x s - (l_x^2 + \pi^2) \frac{s^2 + u^2}{2t}, \end{aligned} \quad (15)$$

and logarithms look like

$$l_s = \log \frac{s}{|t|}, \quad l_x = \log \frac{u}{t}. \quad (16)$$

It should be noted that vertex and box parts contain the infrared divergence through the appearance of the fictitious photon mass λ . The infrared part from virtual cross section can be extracted in a simple way:

$$\begin{aligned} \sigma_{IR}^V &= \sigma^V - \sigma^V(\lambda^2 \rightarrow s) \\ &= -\frac{2\alpha}{\pi} \log \frac{s}{\lambda^2} \left(\log \frac{tu}{m^2 s} - 1 \right) \sigma^0. \end{aligned} \quad (17)$$

B. Real bremsstrahlung contribution

The full set of Feynman graphs contributed to the real photon bremsstrahlung are presented in Fig. 3. For extraction of the infrared divergence we use the prescription of Bardin and Shumeiko [11]:

$$\sigma^R \equiv \sigma^R - \sigma_{IR}^R + \sigma_{IR}^R = \sigma_F^R + \sigma_{IR}^R, \quad (18)$$

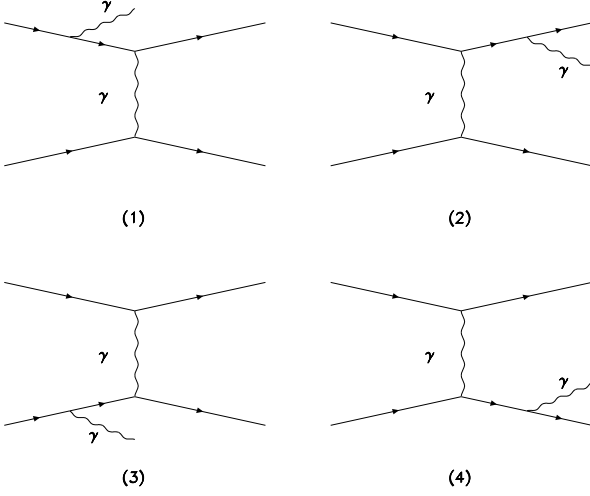


FIG. 3: The real one photon emission graphs giving contribution to the corrected Møller scattering within t -channel.

where the infrared free part can be presented in the following way

$$\sigma_F^R = -\frac{\alpha^3}{\pi s} \int_0^{v_{max}} dv \sum_{i=1}^{10} S_i. \quad (19)$$

The explicit expressions for S_i are presented in the Appendix. The integration in (19) is performed over variable v that is a so-called inelasticity. The reason of this term can be explain by the fact that for the radiative process the last relation in (1) transforms into

$$s + t + u = v + 4m^2. \quad (20)$$

The explicit expression for v can be defined as $v = \Lambda^2 - m^2$, where $\Lambda = k_1 - k_2 + p_1$ and Λ^2 is a so-called missing mass squared.

It should be noted that due to kinematical restrictions the upper limit of the integration in (19) is defined as

$$v_{max} = \frac{st + \sqrt{s(s - 4m^2)t(t - 4m^2)}}{2m^2} \sim s + t. \quad (21) \quad \text{and}$$

From the other side, the energy of the scattering lepton in Lab. system for the radiative process transform from (8) into

$$E_{k_2} = \frac{s + t - v}{2m}, \quad (22)$$

and reaches its minimum value for $v = v_{max}$

$$E_{k_2} = \frac{s + t - v_{max}}{2m} \sim -m \frac{(s - t)^2}{2st}. \quad (23)$$

Obviously the electron with the energy (23) cannot be detected. Moreover, as it was point out first in [13], the variable v can be directly reconstructed from the measured momenta. However not all events with non-zero $v < v_{cut}$ can be rejected from the experimental data due to finite resolution of the experimental equipment. Therefore during the radiative correction calculation for the given experimental setup it is necessary to take into account this fact.

The infrared-divergent part of bremsstrahlung cross section integrated over the real photon phase space is given in terms of a finite (and infinitesimal) photon mass λ in

$$\sigma_{IR}^R = \frac{\alpha}{\pi} \left[4 \log \frac{v_{max}}{m\lambda} \left(\log \frac{tu}{m^2 s} - 1 \right) + \delta_1^S + \delta_1^H \right] \sigma^0, \quad (24)$$

where (see [11] for details)

$$\begin{aligned} \delta_1^S &= -\frac{1}{2} l_m^2 + (3 - 2l_r) l_m - (l_m - 1) \log \frac{s(s+t)}{t^2} - \frac{1}{2} l_r \\ &\quad - \frac{\pi^2}{3} + 1 \end{aligned} \quad (25)$$

$$\begin{aligned} \delta_1^H &= -\frac{5}{2} l_m^2 + \left(\log \frac{t^2(s+t)^2(s-v_{max})}{s(s+t-v_{max})^2 v_{max}(v_{max}-t)} + 1 \right) l_m - \frac{1}{2} \log^2 \frac{v_{max}}{|t|} - \log^2 \left(1 - \frac{v_{max}}{t} \right) \\ &\quad + \log \frac{s+t}{s+t-v_{max}} \log \frac{(s+t)(s+t-v_{max})}{t^2} + \log \frac{s-v_{max}}{|t|} \log \frac{s-v_{max}}{s} + \log \frac{v_{max}}{|t|} \\ &\quad + 2 \left[\text{Li}_2 \left(\frac{v_{max}}{s} \right) - \text{Li}_2 \left(\frac{v_{max}}{t} \right) - \text{Li}_2 \left(\frac{v_{max}}{s+t} \right) \right] + \text{Li}_2 \left(\frac{s-v_{max}}{s} \right) - \text{Li}_2 \left(\frac{t-v_{max}}{t} \right) - \frac{\pi^2}{6} \end{aligned} \quad (26)$$

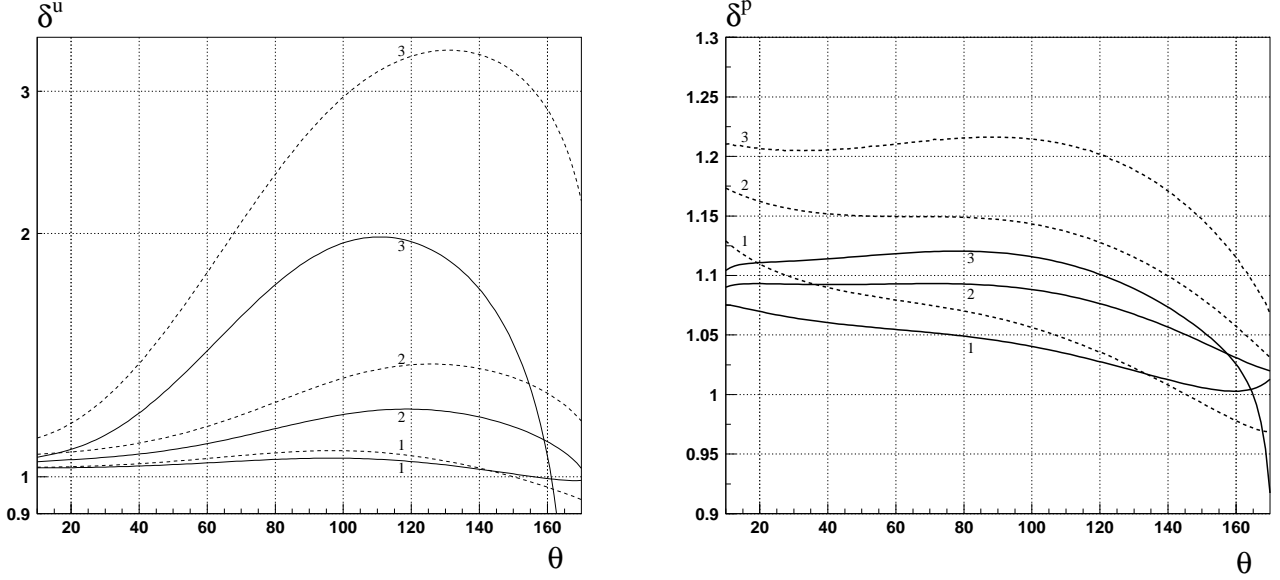


FIG. 4: The relative corrections to the unpolarized (δ^u) and polarized (δ^p) parts of the cross section as a functions of the scattering angle for JLab ($E_{beam} = 1$ GeV, solid lines) and SLAC ($E_{beam} = 45$ GeV, dashed lines) kinematic conditions with different inelasticity cuts: 1) $v_{cut} = 0.5v_{max}$; 2) $0.9v_{max}$; 3) $0.99v_{max}$.

Here $\text{Li}_2(x)$ is the Spence function and

$$l_m = \log \frac{-t}{m^2}, \quad l_r = \log \frac{s+t}{s}, \quad \tau = v + m^2. \quad (27)$$

Summing up (9) and (24)

$$\begin{aligned} \sigma^{RV} &= \sigma_{IR}^R + \sigma^V = \frac{\alpha}{\pi} \left(4 \log \frac{v_{max}}{m\sqrt{s}} \left(\log \frac{tu}{m^2 s} - 1 \right) + \delta_1^S \right. \\ &\quad \left. + \delta_1^H \right) \sigma^0 + \sigma^V(\lambda^2 \rightarrow s), \end{aligned} \quad (28)$$

we obtain a cancellation of infrared divergencies from R- and V- contribution.

Finally, the total infrared free radiative corrected cross section reads:

$$\sigma^{obs} = \sigma^0 + \sigma^{RV} + \sigma_F^R. \quad (29)$$

IV. NUMERICAL ESTIMATIONS

Basing on the equation (29) the FORTRAN code MERA[19] (Møller scattering: Electromagnetic RAdiative corrections) has been developed. In the present section using this code the numerical estimation for radiative effects to the Møller scattering of longitudinally polarized electrons is presented.

There are two basic differences between the numerical analysis that are performed in this and previous [6, 10] papers: we show the dependence of radiative corrections on the scattering angle in the center mass system of the initial electrons, we investigate the dependence of radiative corrections on the value of the missing mass cut.

The cross section for polarized Møller scattering can be presented as a difference of the unpolarized and polarized parts

$$\sigma^{0,obs} = \sigma_u^{0,obs} - P\sigma_p^{0,obs}. \quad (30)$$

In the Fig. 4 the θ -dependence of the relative radiative correction for the unpolarized and polarized parts of the cross section

$$\delta^{u,p} = \sigma_{u,p}^{obs} / \sigma_{u,p}^0 \quad (31)$$

for three different inelasticity cuts v_{cut} (and, therefore Λ^2 cuts): $v_{cut} = 0.5v_{max}$, $0.9v_{max}$ and $0.99v_{max}$ is presented. One can see the following features of their behavior: the presence of maximum values at $\theta \geq 90^\circ$; sizable increasing when v_{cut}^{max} tending to its maximum value. For the $v_{cut} = 0.5v_{max}$ the corrections δ^u (δ^p) for $\theta = 90^\circ$ equal to 1.075 (1.064) for SLAC and 1.054 (1.045) for JLab.

The θ -dependence of the Born and observable asymmetries with the same inelasticity cuts is presented in Fig. 5. In this figure it can be seen that in the most region of θ the corrected asymmetries are less then the Born ones and essentially decrease with the increasing v_{cut} . The Fig. 6, where θ -dependence of the relative corrections to the asymmetries

$$\delta_A = \frac{A_{LR}^{obs} - A_{LR}^0}{A_{LR}^0} \quad (32)$$

is presented, reflects this fact clear. Particularly, it could be seen that for the realistic $v_{cut}^{max} = 0.5v_{max}$ we have $\delta_A = -0.008(-0.01)$ for JLab (SLAC) at $\theta = 90^\circ$ while

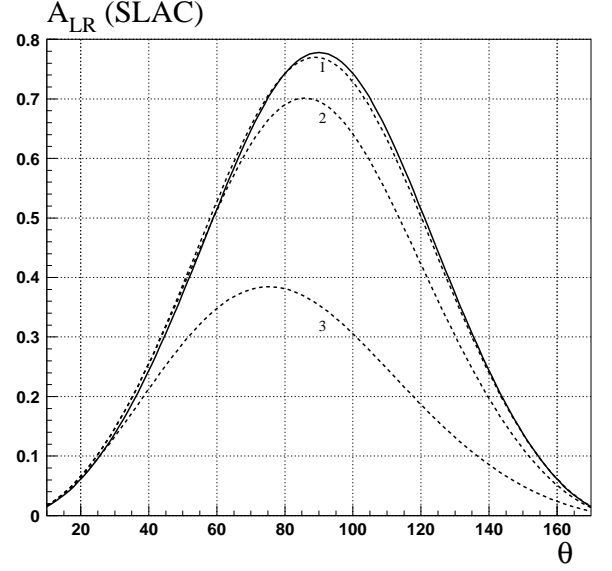
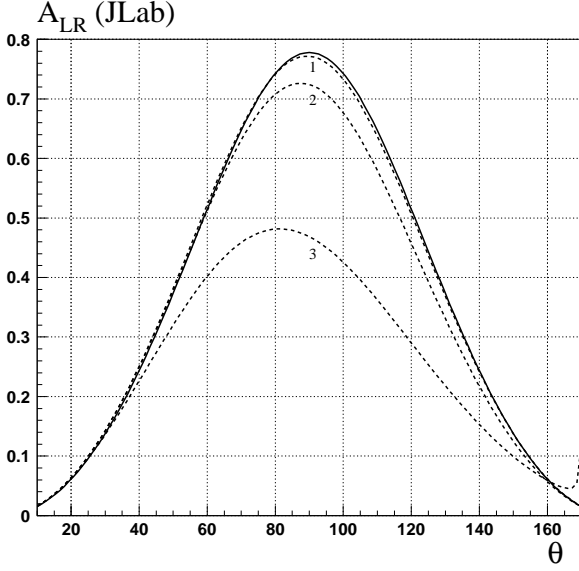


FIG. 5: θ -dependence of the Born (solid line) and observable (dashed lines) asymmetries for JLab ($E_{beam} = 1$ GeV) and SLAC ($E_{beam} = 45$ GeV) kinematic conditions with different inelasticity cuts: 1) $v_{cut} = 0.5v_{max}$; 2) $0.9v_{max}$; 3) $0.99v_{max}$.

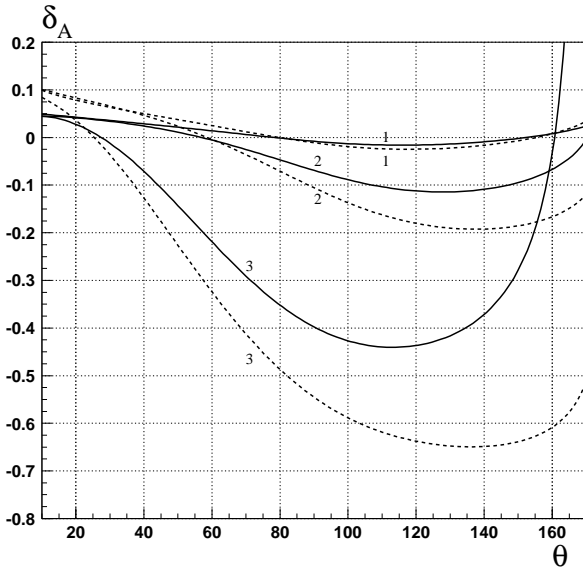


FIG. 6: The relative corrections to the asymmetry (32) as a functions of the scattering angle for JLab ($E_{beam} = 1$ GeV, solid lines) and SLAC ($E_{beam} = 45$ GeV, dashed lines) kinematic conditions with different inelasticity cuts: 1) $v_{cut} = 0.5v_{max}$; 2) $0.9v_{max}$; 3) $0.99v_{max}$.

for $v_{cut}^{max} = 0.99v_{max}$ the relative corrections to the asymmetries reach $\delta_A = -0.4(-0.55)$ for JLab (SLAC) at the same angle.

Now we want to consider the situation with more realistic small v_{cut} . As it could be seen from (26) and (28) the radiative corrected cross section (29) diverge when v_{cut} tends to zero. Such cross section behavior can be explain in a simple way. Naturally that there is no any real photon emission in the limit $v_{cut} \rightarrow 0$. Therefore we

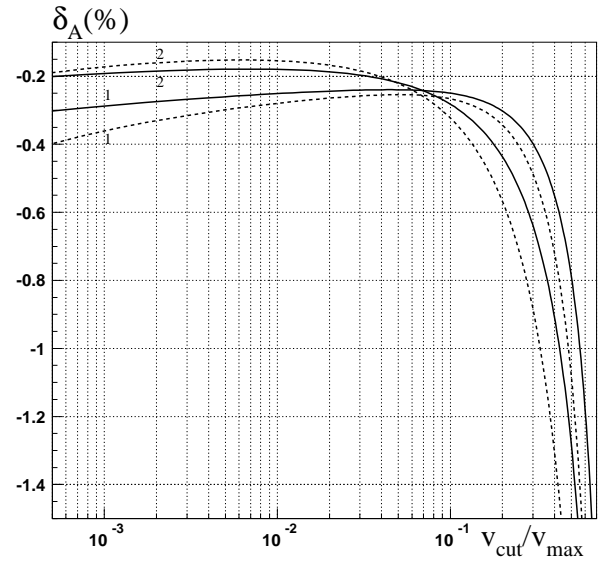


FIG. 7: The relative corrections to the asymmetry (32) as a functions of v_{cut}/v_{max} at the scattering angle in CM system 1) $\theta = 90^\circ$; 2) 100° for JLab ($E_{beam} = 1$ GeV, solid lines) and SLAC ($E_{beam} = 45$ GeV, dashed lines) kinematic conditions.

need to say about the infrared divergency that appear from V-contribution and can not be canceled due to any real photon emission absent.

The other very interesting feature consists in the deviation of the observable asymmetry from the Born one at the small v_{cut} where asymmetry reach its maximum value. Due to rather small effects once again in Fig. 7 the quantity (32) as a function of the ratio v_{cut}/v_{max} is presented for JLab and SLAC kinematic conditions. From this picture it can be seen that for $0.001v_{max} < v_{cut} <$

$0.1v_{max}$ the relative correction to the asymmetry is flat and consists some dozen of percent while starting with $v_{cut} > 0.1v_{max}$ it rapidly falls.

In the end of this section it is necessary to say, that according to agreement between us, Shumeiko and Suarez the comparison of our code MERA [19] with FORTRAN code MØLLERAD [6] is in the progress.

V. CONCLUSIONS

The explicit expressions for the lowest order electromagnetic radiative corrections to Møller scattering of longitudinally polarized electrons in ultrarelativistic approximation have been obtained. Basing on these expressions the FORTRAN code MERA has been developed.

The numerical analysis performed for different values of missing mass (inelasticity) cut has shown that the radiative corrections are strongly depended on this parameter. So when this cut tends to its maximum value two tendencies should be observed: the radiatively corrected cross sections increase while the radiatively corrected asymmetries decrease. At the same time θ -dependence has shown some common features: the relative corrections to the cross sections (asymmetries) has a maximum (minimum) at $\theta \geq 90^\circ$. For more realistic small cuts the relative corrections to the asymmetry are rather flat and

amounts some dozen percent.

Taking into consideration a large scale of obtained radiative effects we proof the necessity of radiative correction procedure for JLab and SLAC experiments. Particularly to perform data processing correctly it is necessary to construct Monte Carlo generator for simulation of radiative events within Møller scattering.

Acknowledgments

The authors would like to thank Andrei Afanasyev, Igor Akushevich, Eugene Chudakov, Yury Kolomensky, Nikolai Shumeiko and Juan Suarez for stimulating discussions. We also thank Nikolai Shumeiko and Juan Suarez for agreement to compare the numerical results from FORTRAN codes MØLLERAD and MERA. V.Z. (A.I) would like to thank SLAC (JLab) staff for their generous hospitality during their visits.

APPENDIX

S_1 is the t -channel contribution of the emission from the upper electron leg:

$$\begin{aligned}
 S_1 &= S_1^u + PS_1^p + S_1^a, \\
 S_1^u &= -L_A - \hat{L}_A + L_s(2s^2t^{-2} + 2t^{-1}u + 2t^{-2}u^2 + 1) + L_x(-2s^2t^{-2} - 2st^{-1} - 2t^{-2}u^2 - 1) - 2L_t + 4L_m \\
 &\quad - 2t^{-2}(v(s^2 + u^2)s^{-1}u^{-1} - 2t), \\
 S_1^p &= -L_A + \hat{L}_A + L_s(-2t^{-1}u - 1) + L_x(-2st^{-1} - 1) + 4L_mt^{-1}(s - u) + 4t^{-2}(s + t - u) \\
 &\quad - 2(4s^2 + 2st - t^2)s^{-1}t^{-1}(s + t)^{-1} - 2(3s + 2t)t^{-1}u^{-1} + 2us^{-1}t^{-1}, \\
 S_1^a &= 4(1 + P)t^{-2}(u + u_0)(1 + tL_m); \tag{A.1}
 \end{aligned}$$

S_2 is the t -channel contribution of the interference from the upper and lower electron legs:

$$\begin{aligned}
 S_2 &= (S_2^u + PS_2^p)/t + S_2^a, \\
 S_2^u &= L_s(8s^3t^{-1} - 8s^2t^{-1}v + 8s^2 + 4st + 4st^{-1}v^2 - 6sv - t^2 + 2tv - v^2)/(t - v) + L_x(-8s^3t^{-1} + 16s^2t^{-1}v \\
 &\quad - 16s^2 - 12st - 12st^{-1}v^2 + 22sv - 5t^2 + 12tv + 4t^{-1}v^3 - 11v^2)/(t - v) + 2L_u(2s + t - v) \\
 &\quad + L_1(4s^3t^{-1} - 4s^2t^{-1}v + 2s^2 + st + 2st^{-1}v^2 - sv + tv - v^2) + L_2(-4s^3t^{-1} + 8s^2t^{-1}v - 10s^2 - 9st \\
 &\quad - 6st^{-1}v^2 + 13sv - 3t^2 + 7tv + 2t^{-1}v^3 - 6v^2) + 2L_3t(-2s - t + v) + 2t((v - s)^{-1} - (s + t)^{-1} \\
 &\quad + 2(2s + t - v)/(t - v)^2),
 \end{aligned}$$

$$\begin{aligned}
S_2^p = & L_s(12s^2t + 8s^2t^{-1}v^2 - 20s^2v + 4st^2 - 12stv - 4st^{-1}v^3 + 12sv^2 - t^3 + 3t^2v - 3tv^2 + v^3)/(t-v)^2 \\
& + L_x(-12s^2t - 8s^2t^{-1}v^2 + 20s^2v - 20st^2 + 52stv + 12st^{-1}v^3 - 44sv^2 - 7t^3 + 25t^2v - 33tv^2 - 4t^{-1}v^4 \\
& + 19v^3)/(t-v)^2 + 2L_ut + L_1(2s^2t^2 - 8s^2tv - 4s^2t^{-1}v^3 + 10s^2v^2 + st^3 - 3st^2v + 5stv^2 + 2st^{-1}v^4 \\
& - 5sv^3 + t^3v - 3t^2v^2 + 3tv^3 - v^4)/(t-v)^2 + L_2(-2s^2t^2 + 8s^2tv + 4s^2t^{-1}v^3 - 10s^2v^2 - 3st^3 \\
& + 17st^2v - 31stv^2 - 6st^{-1}v^4 + 23sv^3 - t^4 + 7t^3v - 17t^2v^2 + 19tv^3 + 2t^{-1}v^5 - 10v^4)/(t-v)^2 - 2L_3tv \\
& - 2t(t+v)(s+t)^{-1}(s-v)^{-1},
\end{aligned}$$

$$S_2^a = 2t^{-2}\{(L_x - \hat{L}_A)(s^2(1-P) + (u^2 + uu_0 + u_0^2)(1+P)) + s(L_A + L_s)(1+P)(u + u_0)\}; \quad (\text{A.2})$$

S_3 is the t -channel contribution of the emission from the lower electron leg:

$$\begin{aligned}
S_3 &= (S_3^u + PS_3^p)/t^2 + S_3^a, \\
S_3^u &= -L_ut(s^2 + u^2)(v-2t)(t-v)^{-2} + (3s^2t^3\tau^{-1} + 12s^2t^2 - 13s^2tv + 4s^2v^2 + 3st^4\tau^{-1} + 9st^3 \\
&\quad - 25st^2v + 17stv^2 - 4sv^3 + \frac{3}{2}t^5\tau^{-1} + t^4 - 13t^3v + 19t^2v^2 - \frac{21}{2}tv^3 + 2v^4)/(t-v)^3, \\
S_3^p &= L_ut(s-u)(2t-v)(t-v)^{-1} + \frac{(s-u)}{2\tau}(st^3 + 8t^2v - 7tv^2 + 4v^3)(t-v)^{-2}, \\
S_3^a &= 2(1+P)t^{-2}(u+u_0)(1+tL_u); \quad (\text{A.3})
\end{aligned}$$

$S_{4,5,6,7}$ are the contributions of the interference between the t - and u -channel graphs:

$$\begin{aligned}
S_4 &= ((1-P)S_4^c + PS_4^p)/u + S_4^a, \\
S_4^c &= -2L_1s^3t^{-1} + L_2(2s^3t^{-1} + 4s^2 + 3st + t^2) + 2\hat{L}_A(-3s^3 - 7s^2t + 2s^2v - 5st^2 + 3stv - t^3 \\
&\quad + t^2v)(s+t)^{-2} + 2L_m(2s-v) + L_sst^{-1}(2s-v) + L_x(-4s^2t^{-1} + 3st^{-1}v - 6s - 3t - t^{-1}v^2 + 3v) \\
&\quad + L_t(-2s - 3t + 2v) + L_3t(2s+t) + 2(-2s^3t^{-1}v + s^3 - 2s^2t - 3st^2 + 3stv - sv^2 \\
&\quad - t^2v + tv^2)(s+t)^{-2}(t-v)^{-1}, \\
S_4^p &= 4s^2t^{-1}v(s+t)^{-2}, \\
S_4^a &= 2s^2(1-P)(2-u_0\hat{L}_A + 2tL_m + sL_A)/(tuu_0); \quad (\text{A.4})
\end{aligned}$$

$$S_5 = (1-P)S_5^c + S_5^a,$$

$$\begin{aligned}
S_5^c &= L_5v + 2L_6(-s^3 - s^2u + s^2v - sv^2 - uv^2 + v^3)(s+u)^{-1}(v-u)^{-1}t^{-1} - \hat{L}_A + 2L_m(-2s^4u^{-1} \\
&\quad + 5s^3u^{-1}v - 4s^3 - 3s^2u - 6s^2u^{-1}v^2 + 10s^2v - 2su^2 + 9suv + 4su^{-1}v^3 - 11sv^2 - u^3 + 4u^2v - 6uv^2 - u^{-1}v^4 \\
&\quad + 4v^3)(s+u)^{-1}(v-u)^{-1}t^{-1} + L_r(-2s^3 - 2s^2u + s^2v - u^2v)(s+u)^{-1}(v-u)^{-1}t^{-1} \\
&\quad + L_s(4s^4u^{-1} - 4s^3u^{-1}v + 4s^3 + 4s^2u + 3s^2u^{-1}v^2 - 8s^2v - 4suv - su^{-1}v^3 + 6sv^2 + 2uv^2 - 2v^3)(s+u)^{-1} \\
&\quad (v-u)^{-1}t^{-1} - L_t + L_u - L_x(4s^3u + 2s^3u^{-1}v^2 - 6s^3v - s^2u^2 + 2s^2uv - s^2v^2 - 2su^3 + 7su^2v - 8suv^2 + 3sv^3 \\
&\quad - u^4 + 3u^3v - 4u^2v^2 + 3uv^3 - v^4)(s+u)^{-1}(u-v)^{-2}t^{-1} + 4(2s-v)u^{-1}t^{-1}, \\
S_5^a &= 2s^2(1-P)(2 + sL_s + 2tL_m + u_0L_x)t^{-1}u^{-1}u_0^{-1}; \quad (\text{A.5})
\end{aligned}$$

$$\begin{aligned}
S_6 &= (1 - P)S_6^c/(tu) + S_6^a, \\
S_6^c &= 2L_u s^2 - 3\tau^{-1}s^2 t^3(t-v)^{-3} + t(5s^4 t - 2s^4 v + 10s^3 t^2 - 4s^3 tv + s^2 t^3 + 10s^2 t^2 v - 12s^2 tv^2 + 4s^2 v^3 - 4st^4 \\
&\quad + 14st^3 v - 18st^2 v^2 + 10stv^3 - 2sv^4 + t^4 v - 3t^3 v^2 + 3t^2 v^3 - tv^4)(s+t)^{-2}(t-v)^{-3} \\
S_6^a &= 2s^2(1 - P)(sL_s - u_0 \hat{L}_A + tL_u)t^{-1}u^{-1}u_0^{-1}; \\
S_7 &= ((1 - P)S_7^c + PS_7^p)/(tu) + S_7^a, \\
S_7^c &= -2L_1 s^3 + L_4 t(s^2 + t^2) + L_5(s+t)(s-t-v)u + L_s s(2s-v) + L_x(-4s^2 - 2st + 3sv + tv - v^2) \\
&\quad + L_u(-3s^2 t^2 + 4s^2 tv - s^2 v^2 - 2st^3 + 6st^2 v - 6stv^2 + 2sv^3 - t^4 + 3t^3 v - 4t^2 v^2 + 3tv^3 - v^4)(t-v)^{-2} \\
&\quad + 2(-4s^3 t + 2s^3 v - 7s^2 t^2 + 5s^2 tv - 3st^3 + 3st^2 v - t^3 v + 2t^2 v^2 - tv^3)(s+t)^{-1}(t-v)^{-2}, \\
S_7^p &= 4s^{-1}v(s^3 + 2t^2 v - 4tv^2 + 2v^3)(t-v)^{-2}, \\
S_7^a &= 2s^2(1 - P)(2 + u_0 L_x + tL_u + sL_A)t^{-1}u^{-1}u_0^{-1};
\end{aligned} \tag{A.6}$$

$S_{8,9,10}$ are the pure u-channel contributions:

$$\begin{aligned}
S_8 &= (S_3^u + PS_3^p)|_{t \leftrightarrow u}/u^2 + S_8^a, \\
S_8^a &= -2(s^2 + t^2 - (s^2 - t^2)p)((u + u_0)u^{-2}u_0^{-2} \\
&\quad - \hat{L}_A u^{-1}u_0^{-1}); \\
S_9 &= (S_2^u + PS_2^p)|_{t \leftrightarrow u}/u + S_9^a, \\
S_9^a &= -2(s^2 + t^2 - (s^2 - t^2)p)(2tL_m + sL_A + sL_s \\
&\quad + tL_u)(u + u_0)u^{-2}u_0^{-2}; \\
S_{10} &= (S_1^u + PS_1^p)|_{t \leftrightarrow u} + S_{10}^a, \\
S_{10}^a &= -2(s^2 + t^2 - (s^2 - t^2)p)(2(u + u_0)u^{-2}u_0^{-2} \\
&\quad + L_x u^{-1}u_0^{-1});
\end{aligned} \tag{A.8}$$

Evidently, the contributions S_1 , S_2 , S_3 are in agreement with the corresponding terms of calculations [17] (unpolarized fermion scattering) and [18] (longitudinally polarized fermion scattering), if we suppose that masses of the initial fermions being equal.

Here we present the logarithms (and their combinations) which were used in hard bremsstrahlung calculation (notice that all of them do not lead to infrared singularity):

$$\begin{aligned}
L_m &= -\frac{1}{t} \log \frac{|t|}{m^2}, \quad L_A = -\frac{1}{v-s} \log \frac{(v-s)^2}{m^2 \tau}, \\
\hat{L}_A &= -\frac{1}{v-u} \log \frac{(v-u)^2}{m^2 \tau}, \quad L_t = \frac{1}{v-t} \log \frac{\tau(v-t)^2}{m^2 t^2}, \\
L_s &= \frac{1}{s} \log \frac{s^2}{m^4}, \quad L_x = -\frac{1}{u} \log \frac{u^2}{m^4}, \\
L_u &= \frac{1}{v-t} \log \frac{(v-t)^2}{m^2 \tau}, \quad L_1 = \frac{1}{v}(L_s - L_A), \\
L_2 &= \frac{1}{v}(L_x + \hat{L}_A), \quad L_3 = \frac{1}{v}L_t, \\
L_4 &= \frac{1}{v}(L_u - 2L_m), \quad L_5 = \frac{1}{v(s+t)} \log \frac{u^2 m^2}{(v-u)^2 \tau}, \\
L_6 &= \frac{1}{s} \log \frac{s\tau^2}{m^2 ut}, \quad L_r = \frac{1}{u} \log \frac{t^2}{u^2}.
\end{aligned} \tag{A.11}$$

[1] K.S.Kumar et al., Mod. Phys. Lett. **A10**, 2979 (1995).
[2] P. Anthony et al., Phys. Rev. Lett **92**, 181602 (2004).
[3] G. Alexander and I. Cohen, Nucl. Instrum. Meth. **A486**, 552 (2002).
[4] T. Benisch et al., Nucl. Instrum. Meth. **A471**, 314 (2001).

[5] C.A.Heusch, Int. J. Mod. Phys **A15**, 2347 (2000).
[6] N. Shumeiko and J. Suarez, J. Phys. **G6**, 113 (2000).
[7] A. Denner and S. Pozzorini, Eur. Phys. J. **C7**, 185 (1999).
[8] A. Czarnecki and W. Marciano, Phys. Rev. **D53**, 1066 (1996).
[9] F.J.Petriello, Phys. Rev. **D67**, 033006 (2003).

- [10] V. Zykunov, Yad. Fiz. **67**, 1366 (2004).
- [11] D. Bardin and N. Shumeiko, Nucl. Phys. **B127**, 242 (1977).
- [12] N. Shumeiko, Sov. J. Nucl. Phys. **29**, 969 (1979).
- [13] I. Akushevich, Eur. Phys. J. **C8**, 457 (1999).
- [14] A. Afanasev et al., Phys. Rev. **D66**, 074004 (2002).
- [15] M. Böhm et al., Fortschr. Phys. **34**, 687 (1986).
- [16] H. Burkhard and B. Pietrzyk, Phys. Lett. **B356**, 398 (1995).
- [17] D. Bardin and N. Shumeiko (1977), JINR P2-10872.
- [18] V. Zykunov et al., Yad. Fiz. **58**, 2021 (1995).
- [19] FORTRAN code MERA is available from <http://www.hep.by/RC>